Assembly Dynamics and Detailed Structure of 1-Propanethiol Monolayers on Au(111) Surfaces Observed Real Time by in situ STM

ARTICLE *in* LANGMUIR · AUGUST 2006

Impact Factor: 4.46 · DOI: 10.1021/la0605891 · Source: PubMed

3 AUTHORS, INCLUDING:

Jingdong Zhang
Technical University of Denmark
101 PUBLICATIONS **2,318** CITATIONS

SEE PROFILE

Qijin Chi
Technical University of Denmark
101 PUBLICATIONS **2,315** CITATIONS

SEE PROFILE

Assembly Dynamics and Detailed Structure of 1-Propanethiol Monolayers on Au(111) Surfaces Observed Real Time by in situ STM

Jingdong Zhang,* Qijin Chi, and Jens Ulstrup

Department of Chemistry and NanoDTU, Building 207, Technical University of Denmark, DK-2800 Kgs. Lyngby, Denmark

Received March 3, 2006. In Final Form: April 25, 2006

1-Propanethiol is chosen as a model alkanethiol to probe detailed mechanisms of the self-assembled monolayer (SAM) formation at aqueous /Au(111) interfaces. The assembly processes, including initial physi- and chemisorption, pit formation, and domain growth, were recorded into movies in real-time with high resolution by in situ scanning tunneling microscopy (STM) under potential control. Two major adsorption steps were disclosed in the propanethiol SAM formation. The first step involves weak interactions accompanied by the lift of the Au(111) surface reconstruction, which depends reversibly on the electrochemical potentials. The second step is chemisorption to form a dense monolayer, accompanied by formation of pits as well as structural changes in the terrace edges. Pits emerged at the stage of the reconstruction lift and increased to a maximum surface coverage of 4.0 ± 0.4% at the completion of the SAM formation. Well-defined triangular pits in the SAM were found on the large terraces (more than 300 nm wide), whereas few and small pinholes appeared at the terrace edge areas. Smooth edges were converted into saw-like structural features during the SAM formation, primarily along the Au(111) atomic rows. These observations suggest that shrinking and rearrangement of gold atoms are responsible for both formation of the pits and the shape changes of the terrace edges. STM images disclose a $(2\sqrt{3} \times 3)R30°$ periodic lattice within the ordered domains. Along with electrochemical measurements, each lattice unit is assigned to contain four propanethiol molecules exhibiting different electronic contrasts, which might originate in different surface orientations of the adsorbed molecules.

Introduction

Self-assembled monolayers (SAMs) based on sulfur−metal interactions have long attracted attention due to fundamental interest in surface phenomena as well as wide applications in surface molecular architecture, corrosion prevention, molecular devices, and nanoscale fabrication.[1,2] Alkanethiol monolayers on gold surfaces are among the most extensively investigated systems. This is due to the chemically inert nature of gold itself and to the specific strong interactions between gold and sulfur. In addition, extension to branched or adamantane-based thiols and alkanethiols with tailored functional end groups could provide entirely new SAM classes with other chemical and physical properties.[3] Such SAM-modified surfaces can be used to immobilize biological macromolecules with their electron transfer (ET) or enzyme function retained.[4−10]

Two major approaches have been frequently used in the preparation of thiol SAMs. One is based on "dry" methods, i.e., gas-phase deposition similar to evaporation techniques in ultrahigh vacuum (UHV).[11,12] The advantage is that thiol monolayers are grown in a clean environment and that a large number of UHV-based tools can be used for structural and functional characterization. The other method is the "wet" (or solution) approach where the SAMs are formed spontaneously by immersing clean gold substrates in a thiol-containing solution with a suitable concentration. This approach is attractive first because of easy operation and low cost. The operation of the "wet" method in environments close to normal chemical or biological conditions, moreover, makes it particularly appealing for biological applications of SAMs. It is obvious that the environments for thiol assembly are drastically different in the "dry" and "wet" methods. Although similar steady-state structures in UHV and solution are reported for some alkanethiols,[11,13] significant differences in molecular packing and surface lattice structures were observed, for example for cysteine monolayers in UHV[14] and in solution.[15,16] This suggests that solvent effects, ionic interactions, and hydrogen bonds play crucial roles in the monolayer formation and the final steady surface structures.[17]

Many techniques have been employed to characterize thiol SAMs. Overviews of recent progress are given by Ulman[18] and Schreiber.[19] Electronic spectroscopies, scanning probe microscopies (SPM) including STM and atomic force microscope (ATM), and other surface-sensitive techniques have provided

* Corresponding author. E-mail: jz@kemi.dtu.dk.

(1) (a) Love, J. C.; Estroff, L. A.; Kriebel, J. K.; Nuzzo, R. G.; Whitesides, G. M. *Chem. Rev.* **2005**, *105*, 1103−1169. (b) Lahann, J.; Mitragotri, S.; Tran, T.; Kaido, H.; Sundaram, J.; Choi, I. S.; Hoffer, S.; Somorjai, G. A.; Langer, R. *Science* **2003**, *299*, 371−374.

(2) Smith, R. K.; Lewis, P. A.; Weiss, P. S. *Prog. Surf. Sci.* **2004**, *75*, 1−68.

(3) Dameron, A. A.; Charles, L. F.; Weiss, P. S. *J. Am. Chem. Soc*. **2005**, *127*, 8697−8705.

(4) Kasemo, B. *Surf. Sci.* **2002**, *500*, 656−677.

(5) Gilardi, G.; Fantuzzi, A. *Trends Biotechnol.* **2001**, *19*, 468−476.

(6) (a) Zhang, J.; Chi, Q.; Kuznetsov, A. M.; Hansen, A. G.; Wackerbarth, H.; Christensen, H. E. M.; Andersen, J. E. T.; Ulstrup, J. *J. Phys. Chem. B* **2002**, *106*, 1131−1152. (b) Chi, Q.; Zhang, J.; Jensen, P. S.; Christensen, H. E. M.; Ulstrup, J. *Faraday Discuss.* **2006**, *131*, 181−195.

(7) (a) Avila, A.; Gregory, B. W.; Niki, K.; Cotton, T. M. *J. Phys. Chem. B* **2000**, *104*, 2759−2766. (b) Wei, J.; Niki, K.; Margoliash, E.; Waldeck, D. H.; *J. Phys. Chem. B* **2004**, *108*, 16912−16917.

(8) (a) Chi, Q.; Zhang, J.; Andersen, J. E. T.; Ulstrup, J. *J. Phys. Chem. B* **2001,** *105*, 4669−4679. (b) Chi, Q.; Farver, O.; Ulstrup, J. *Proc. Natl. Acad. Sci. U.S.A.* **2005**, *102*, 16203−16208.

(9) Fujita, K.; Nakamura, N.; Ohno, H.; Leigh, B. S.; Niki, K.; Gray, H. B.; Richards, J. H. *J. Am. Chem. Soc.* **2004**, *126*, 13954−13962.

(10) Zhang, J.; Welinder, A. C.; Hansen, A. G.; Christensen, H. E. M.; Ulstrup, J. *J. Phys. Chem. B* **2003**, *107*, 12480−12484.

(11) Poirier, G. E. *Chem. Rev.* **1997**, *97*, 1117−1127.

(12) Schreiber, F. *Prog. Surf. Sci.* **2000**, *65*, 151−256.

(13) Gewirth, A. A.; Niece, B. K. *Chem. Rev.* **1997**, *97*, 1129−1162.

(14) Kuhnle, A.; Linderoth, T. R.; Hammer, B.; Besebhacher, F. *Nature* **2002**, *415*, 891−893.

(15) Zhang, J.; Chi, Q.; Nielsen, J. U.; Friis, E. P.; Andersen, J. E. T.; Ulstrup, J. *Langmuir* **2000**, *16*, 7229−7237.

(16) Xu, Q. M.; Wan, L. J.; Wang, C.; Bai, C. L.; Wang, Z. Y.; Nozawa, T.; *Langmuir* **2001**, *17*, 6203−6206.

(17) Zhang, J.; Biliæ, A.; Reimers, J. R.; Hush, N. S.; Ulstrup, J. *J. Phys. Chem. B* **2005**, *109*, 15355−15367.

(18) Ulman, A. *Chem. Rev.* **1996**, *96*, 1533−1566.

(19) Duwez, A. S. *J. Electron Spectrosc.* **2004**, *134*, 97−138.

10.1021/la0605891 CCC: $33.50
Published on Web 05/28/2006

structural information of SAMs at the nanoscale and molecular levels.[11,19] In contrast to a large body of literature on steady-state structural features of either ordered or disordered phases of SAMs, studies of dynamic SAM properties are rare, especially for solution SAMs.[12,20] Dynamic investigations of thiol monolayer assembly dynamics are therefore highly desirable. Poirier and co-workers used UHV−STM with gas-phase transport of alkanethiol vapor on clean Au(111) and studied the evolution of several thiol (e.g., mercaptohexanol, octanethiol, and decanethiol) monolayers.[21−26] Focus was on coverage-dependent phases, phase stability, and formation of gold vacancy islands (VIs) in order to disclose self-assembly mechanisms.[21−26] According to observations by real-time UHV−STM, the Au(111) surface in fact exhibits a highly dynamic character when interacting with adsorbed sulfur.[27] Controlling parameters for dry assembly are pressure, time, and temperature, whereas thiol concentration, solvent type, adsorption time, and electrochemical potential of the gold substrate are key parameters for the solution method. Room temperature is suitable for preparation of many thiol monolayers, but temperature annealing can also affect molecular packing.[28] Temperature is not often regarded as a key parameter for the wet method, because temperature variation is limited by evaporation of both solvent and thiols and decomposition of thiols. The electrochemical potential of the gold substrate has instead crucial effects on the stability and structure of SAMs. Electrochemistry has been used extensively to investigate interfacial ET phenomena.[29] Particularly, the Au−S bond in thiol SAMs can be broken by either oxidative or reductive desorption.[30]

In situ STM under potential control offers a unique opportunity to characterize microscopic features of liquid /solid interfaces at the atomic or molecular level.[13,31] In situ STM offers not only steady-state but also dynamic approaches, especially for potential-dependent phenomena.[32,33] This technique has previously been used to monitor the time-dependent assembly of decanethiol on Au(111) in heptane solution[34,35] and dynamic surface structure transitions of dodecanethiol SAMs on Au(111).[36] Reductive desorption processes of several alkanethiol SAMs in 0.5 M KOH solution have, for example, been followed,[37] and both reductive desorption and oxidative adsorption of hexanethiol monolayers on Au(111) in the same medium were recently imaged.[38] Potential-dependent surface structure transitions with accompanying sharp capacitive voltammetric peaks in homocysteine monolayers were further discovered.[33] The transitions showed a highly ordered lattice around the peak potential and disordered structure at either side of this potential.

With a view of more detailed mapping of general dynamic features of the self-assembly of a broad functionalized alkanethiol class, the present study addresses monolayer formation of a short alkanethiol, i.e., 1-propanethiol, using in situ STM and electrochemistry. A short-chain alkanethiol is chosen, because of its relatively high solubility in aqueous buffer solutions (in the ca. mM range) and the monolayers are formed easily within relative short time. Dynamic observations of 1-propanethiol SAMs can therefore be recorded in desired aqueous environments. This provides a solid basis for further investigations of proteins immobilized on the alkanethiol SAMs. The major objective is to characterize detailed structures and dynamic features of the 1-propanethiol SAM. The particular focus is on the time- and potential-dependent evolution of the SAM formation. High-resolution in situ STM mapping has thus enabled us to provide new insight into several fundamental issues of the SAM formation and structure, such as the mechanism of pit formation, relative electronic contrasts, and detailed lattice structure.

Experimental Section

Chemicals. 1-Propanethiol ($CH_3CH_2CH_2SH$) (molecular structure Figure S1) (> 99%) was from Aldrich and used without further purification. The NH_4Ac (5 mM, pH 4.6) buffer solution was prepared from 5 M stock solution (Fluka, ultrapure), and the solution pH was adjusted by acetic acid (99.7%, Aldrich). NaOH (0.5 M) used in reductive desorption measurements was prepared from 30% NaOH (Suprapur, Merck), and Millipore water (18.2 MΩ) was used throughout.

Instrumentation and Procedures. Au(111) electrodes for both electrochemistry and STM were homemade from polycrystalline gold wire (99.99%) according to Hamelin's method.[39−41] The quality of the Au(111) substrates was checked by STM and electrochemistry prior to use. The hanging meniscus method was used for the electrochemistry of the Au(111) electrodes. Electrochemical measurements including cyclic voltammetry, linear scan voltammetry, and capacitance data were carried out using an Eco Chemie Autolab potentiostat (The Netherlands) controlled by the General Purpose Electrochemical system software and frequency response analyzer. A 20 mV step, 5 mV amplitude and 100 Hz frequency were applied in the capacitance measurements. A bright platinum wire was used as the counter electrode, and a freshly prepared reversible hydrogen electrode (RHE) filled with the same supporting electrolyte solution as the reference electrode. The potential of the RHE was checked vs a saturated calomel electrode (SCE) after each measurement. All electrode potentials are referred to SCE. Electrolyte solutions were deoxygenated for several hours by Ar (5N in purity) which was further purified by a Chrompack Gas-clean Oxygen Filter (Varian) before measurements.

A Pico SPM instrument (Molecular Imaging Co., USA) was used for in situ STM imaging. Tungsten or Pt/Ir (80:20) tips were electrochemically etched and insulated by Apiezon wax as previously reported.[17] Homemade PTFE cells (3 mL volume) were used. All images were obtained in the constant current mode.

Glassware, the STM and electrochemical cells, and other related utensils were cleaned as previously reported.[42,43]

Sample Preparation. Before use, the Au(111) electrodes were first treated by electrochemical polishing in 0.1 M H_2SO_4 solution followed by washing in 1 M HCl solution and Millipore water and

(20) Badia, A.; Lennox, R. B.; Reven, L. *Acc. Chem. Res.* **2000**, *33*, 475−481.
(21) Poirier, G. E.; Tarlov, M. J. *Langmuir* **1994**, *10*, 2853−2856.
(22) Poirier, G. E.; Pylant, E. D. *Science* **1996**, *272*, 1145−1148.
(23) Poirier, G. E. *Langmuir* **1997**, *13*, 2019−2026.
(24) Poirier, G. E. *Langmuir* **1999**, *15*, 1167−1175.
(25) Poirier, G. E.; Fitts, W. P.; White, J. M. *Langmuir* **2001**, *17*, 1176−1183.
(26) Fitts, W. P.; White, J. M.; Poirier, G. E. *Langmuir* **2002**, *18*, 1561−1566.
(27) Biener, M. M.; Biener, J.; Friend, C. M. *Langmuir* **2005**, *21*, 1668−1671.
(28) Yamada, R.; Wano, H.; Uosaki, K. *Langmuir* **2000**, *16*, 5523−5525.
(29) Bard, A. J.; Faulkner, L. R. *Electrochemical Methods Fundamentals and Applications*, 2nd ed.; John Wiley & Sons Inc.: New York, 2001.
(30) (a) Yang, D.; Morin, M. *J. Electroanal. Chem.* **1998**, *441*, 173−181. (b) Yang, D.; Wild, C. P.; Morrin, M. *Langmuir* **1997**, *13*, 243−249.
(31) (a) Kolb, D. M. *Prog. Surf. Sci.* **1996**, *51*, 109−173. (b) Roelfs, B.; Bunge, E.; Schroter, C.; Solomun, T.; Meyer, H.; Nichlos, R. J.; Baumgartel, H. *J. Phys. Chem. B* **1997**, *101*, 754−765. (c) Itaya, K. *Prog. Surf. Sci.* **1998**, *58*, 121−248.
(32) Yang, L. O.; Yau, S.; Itaya, K. *Langmuir* **2004**, *20*, 4596−4603.
(33) Zhang, J.; Demetriou, A.; Welinder, A. C.; Albrecht, T.; Nichols, R. J.; Ulstrup, J. *Chem. Phys.* **2005**, *319*, 210−221.
(34) Yamada, R.; Uosaki, K. *Langmuir* **1997**, *13*, 5718−5221.
(35) Yamada, R.; Uosaki, K. *Langmuir* **1998**, *14*, 855−861.
(36) Arce, F. T.; Vela, M. E.; Salvarezza, R. C.; Arvia, A. J. *J. Chem. Phys.* **1998**, *109*, 5703−5706.
(37) Hobara, D.; Miyake, K.; Imabayashi, S.; Niki, K.; Kakiuchi, T. *Langmuir* **1998**, *14*, 3590−3596.
(38) Wano, H.; Uosaki, K. *Langmuir* **2005**, *21*, 4024−4033.
(39) Hamelin, A. *J. Electroanal. Chem.* **1996**, *401*, 1−16.
(40) Sawaguchi, T.; Yamada, Y.; Okinaka, Y.; Itaya, K. *J. Phys. Chem.* **1995**, *99*, 14149−14155.
(41) Zhang, J.; Christensen, H. E. M.; Ooi, B. L.; Ulstrup, J. *Langmuir* **2004**, *20*, 10200−10207.
(42) Chi, Q.; Zhang, J.; Friis, E. P.; Andersen, J. E. T.; Ulstrup, J. *Electrochem. Commun.* **1999**, *1*, 91−96.
(43) Chi, Q.; Zhang, J.; Nielsen, J. U.; Friis, E. P.; Chorkendorff, I.; Canters, G. W.; Andersen, J. E. T.; Ulstrup, J. *J. Am. Chem. Soc.* **2000**, *122*, 4047−4055.

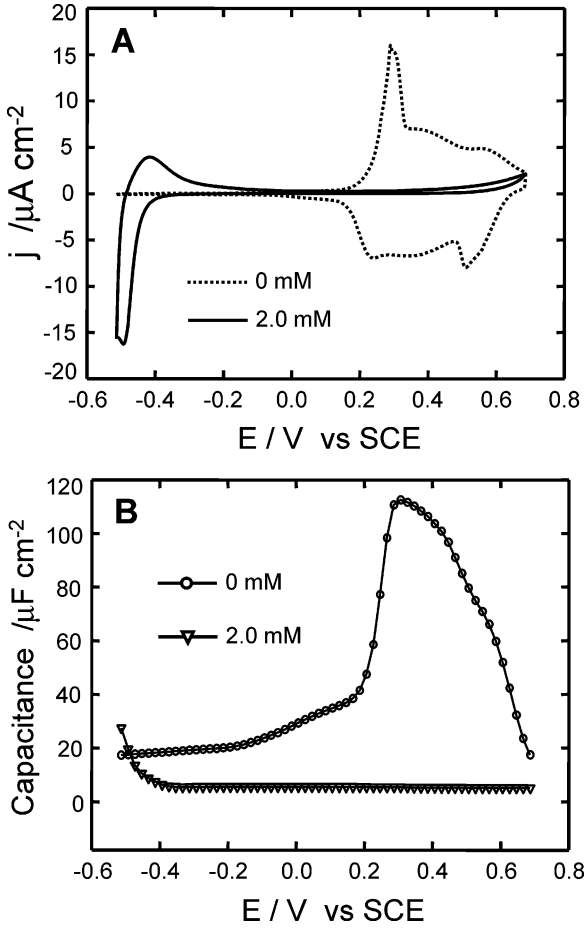

Figure 1. (A) Cyclic voltammetric and (B) capacitance curves of bare Au(111) and 1-propanethiol covered Au(111) electrodes in NH_4Ac buffer (5 mM, pH 4.6). The concentrations of 1-propanethiol in the solution are 0 mM (dotted lines in the voltammogram and empty circles for the capacitance) and 2 mM (solid lines for the voltammogram and triangles for the capacitance). Scan rate 50 mV s^{-1} in voltammetry. Potential step 20 mV, potential amplitude 5 mV, frequency 100 Hz applied in the capacitance measurements.

annealed at 860 °C for 6−8 h. The Au(111) electrodes were further cleaned by a hydrogen flame and quenched in Millipore water saturated by H_2. The Au(111) electrodes were then either transferred to the electrochemical cell or the in situ STM cell under potential control or incubated in 0.5−2 mM 1-propanethiol solutions for several hours.

Results

Electrochemical Measurements. Figure 1 shows cyclic voltammograms (A, dotted lines) and capacitance data (B, circles) of bare Au(111) in NH_4Ac buffer. Both sets of data show a featureless double-layer region between −0.50 and +0.15 V and a sharp anodic peak at +0.3 V. The anodic peak at +0.3 V is caused by the lift of the Au(111) reconstruction and adsorption of acetate anions.[15]

Decay of the anodic peak at +0.30 V is observed in the presence of 1-propanethiol at relatively low concentrations (e.g., 0.5 mM), and an additional cathodic peak appears at −0.50 V. When the concentration of 1-propanethiol is increased to 1.8 mM or higher, the anodic peak at +0.30 V has completely vanished, leaving a wide double-layer region from −0.30 to +0.7 V. Meanwhile, a strong cathodic peak at −0.50 V and a small corresponding anodic peak at −0.43 V have emerged (Figure 1A, solid lines). A similar pattern is featured in the capacitance curve (Figure 1B, triangles). The presence of 2.0 mM 1-propanethiol causes a decrease of the capacitance from 20 μF cm^{-2} of bare Au(111) to 5 μF cm^{-2} (Figure 1B). This is in contrast to hydrophilic monolayers consisting of cysteine or azurin where adsorption of the target molecules gave an increase in the capacitance.[15,42,43] The difference is attributed to the hydrophobic features of the 1-propanethiol SAM surface, even though the alkane chain is very short. The cathodic and anodic peaks at negative potentials (−0.40 to −0.50 V) are caused by reductive desorption of the SAM and partial readsorption of liberated 1-propanethiol, respectively. We found that a dense SAM can be formed only at relatively high concentration (≥0.5 mM) of 1-propanethiol. In contrast, Uosaki and co-workers showed that a much lower thiol concentration (such as 0.3 μM decanethiol in heptane or 1 μM hexanethiol in 20 mM KOH-containing ethanol) could lead to assembly of a full monolayer on Au(111).[34,35,38] No significant adsorption could, however, be detected by either electrochemistry or STM within the observed time scale (a few hours) at 1-propanethiol concentrations below 0.1 mM. A difference in thiol concentration of 2 or 3 orders of magnitude between 1-propanethiol and hexanethiol (or decanethiol) is likely due to the difference in the alkane chain length and the different solvents and supporting electrolytes. The most suitable concentration of 1-propanethiol for dynamic observations in the present case is the range of 0.5−2.0 mM.

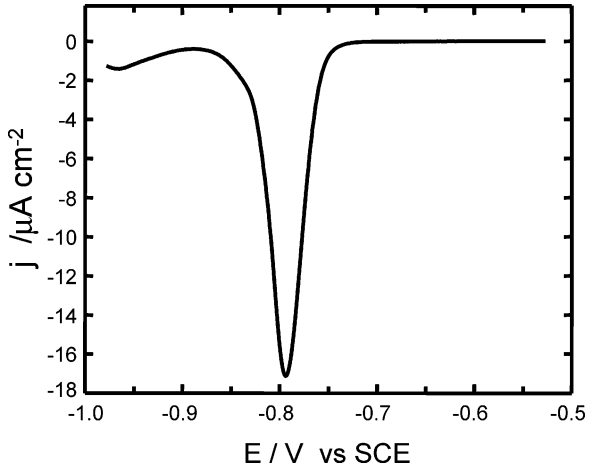

Figure 2. Linear scan voltammogram of the 1-propanethiol SAM on Au(111) in 0.5 M NaOH. Scan rate 10 mV s^{-1}.

The properties and surface coverage of the 1-propanethiol SAMs can be further evaluated by electrochemical reductive desorption in basic solution according to the following reaction:

$$\text{Au-S-CH}_2\text{-CH}_2\text{-CH}_3 + e^- \rightarrow \text{Au} + {}^-\text{S-CH}_2\text{-CH}_2\text{-CH}_3 \quad (1)$$

A uniform SAM with a single surface lattice will give a sharp cathodic peak, whereas multiple phases or configurations in the SAM can result in multiple or even asymmetric peaks.[19,44−46] The peak potential is directly related to the strength of the Au−S bond which is determined by the chain length of the alkanethiol and the chemical properties (e.g., hydrophobic or hydrophilic) of the terminal groups.[9,44] The Faradaic charge under the cathodic peak corresponds to the population of Au−S bonds and is used to estimate the thiol coverage. Figure 2 shows a representative

(44) Widrig, C. A.; Chung, C.; Porter, M. C. *J. Electroanal. Chem.* **1991**, *310*, 335−359.
(45) Imabayashi, S.; Iida, M.; Hobara, D.; Feng, Z. Q.; Niki, K.; Kakiuchi, T. *J. Electroanal. Chem.* **1997**, *428*, 33−38.
(46) Hobara, D.; Ota, M.; Imabayashi, S.; Niki, K.; Kakiuchi, T. *J. Electroanal. Chem.* **1998**, *444*, 113−119.

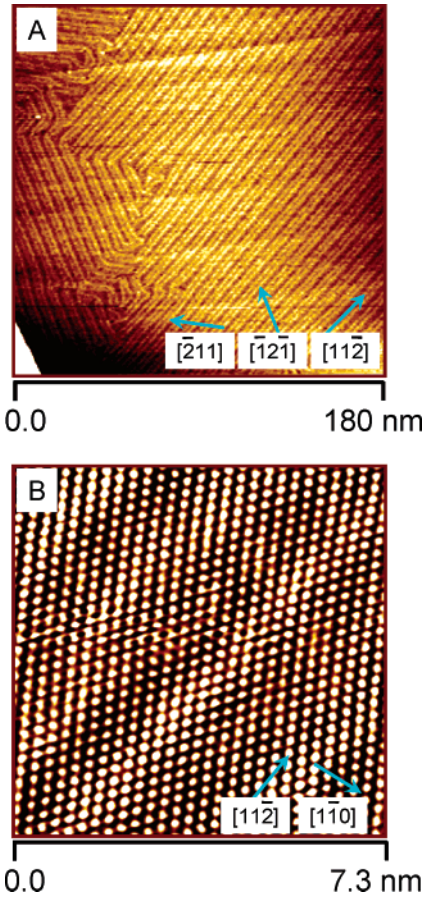

Figure 3. In situ STM images of bare Au(111) in NH_4Ac buffer (5 mM, pH 4.6). Scan area: (A) 180 × 180 nm^2 and (B) 7.3 × 7.3 nm^2. (A) I_t = 0.08 nA, V_{bias} = 0.19 V, E_w = −0.30 V (vs SCE). (B) I_t = 0.80 nA, V_{bias} = 0.05 V, E_w = −0.10 V (vs SCE).

linear scan voltammogram of 1-propanethiol SAMs in 0.5 M NaOH solution with a sharp cathodic peak at −0.79 V. The peak potential is ≈80 mV more negative than for the SAM of similar-size cysteamine terminated with a strongly hydrophilic amine group.[17] This observation is expected when compared with previous studies.[44−46] No peak splitting is observed, implying that only a single surface phase or lattice is present in the 1-propanethiol SAMs. The surface coverage is estimated to be 7.6 (± 0.5) × 10^{-10} mol cm^{-2} by integration of the peak charge and agrees with those for butanethiol[15] and hexadecanethiol.[47] The reductive desorption, however, only discloses steady-state features of 1-propanthiol SAMs, but tracking of the assembly dynamics has been feasible by in situ STM, as described below.

In Situ STM Observations. *The Surface Reconstruction and Structure of Au(111).* The cleanness of the solutions and operating environments was critically controlled in order to achieve reliable in situ observations, as any contaminations would cause uncertain adsorption on the Au(111) surfaces. Figure 3 shows representative STM images of bare Au(111) in NH_4Ac buffer (5 mM, pH 4.6). Herringbone-like lines are clearly observed in the potential range from −0.50 to +0.10 V (Figure 3A). Such a pattern originates in surface reconstruction and is a signature of a clean Au(111) surface.[48] The angles between the reconstruction lines are 60° or multiples of this value, reflecting the 3-fold symmetry of the Au(111) surface. The distance between the nearest neighbor lines is 6.35 nm, corresponding to 23 gold atoms in the top layer located on the second layer occupied by 22 gold atoms. Herringbone-like reconstruction on the Au(111) surface is therefore described as a ($\sqrt{3}$ × 23)R30° super lattice structure.[11] Generally, the longer the ordered reconstruction lines, the better the surface quality of Au(111). The high-resolution STM images were acquired under such reconstruction conditions. An example is shown in Figure 3B. The STM image (Figure 3B) shows typical structural features of the Au(111) surface, i.e., a hexagonal lattice with a periodic distance of 2.8 ± 0.3 Å corresponding to the size of single gold atoms. According to both theoretical analysis and experimental measurements,[11] gold atoms in the reconstructed state should exhibit an elliptical shape with the short axis ca. 4% smaller than the long axis. The elliptical shape of gold atoms is hardly resolved, however, because the resolution required is at the limit of what can be achieved by STM. The atomically resolved images further illustrate that the Au(111) atomic rows such as [1$\bar{1}$ 0] are either oriented by 30° or perpendicular relative to the reconstruction lines (i.e., [11 $\bar{2}$]). These images are used for calibration of STM scanners and serve as a starting platform for dynamic investigations of the 1-propanethiol SAM formation.

Formation of 1-Propanethiol SAMs within Large Au(111) Terraces. We first focus on the SAM formation on the large terraces that are more than 300 nm wide. The STM images were recorded as a function of potential and adsorption time at a relatively high concentration of 1.8 mM 1-propanethiol. A series of such images generating a movie is shown in Figure 4 and follow the evolution during the SAM formation. Figure 4A shows a representative pattern at a very early stage, in which the reconstruction lines have started to lift at −0.48 V by the presence of 1-propanethiol. At this initial stage, an observable feature is the appearance of some patches with weak electronic contrast (for simplicity, we term these as "dark" patches). The patches emerge first in the areas of the joints (or "elbows") between two or three reconstruction lines, as indicated by the black arrows 1 and 2 in Figure 4A. The patches exhibit clearly an equi-triangular shape along the {11$\bar{2}$} directions (i.e., $\sqrt{3}$ directions). Corresponding changes when the substrate potential was shifted slightly positively to −0.45 V are recorded in Figure 4, panels B and C. The most conspicuous change is an expansion in the area of the dark patches, indicated by the black arrows 1, 2 and 3 in Figure 4C. In addition, some new patch sites emerge from the elbows (e.g., the black arrows 4 and 5 in Figure 4C). A similar pattern is found when the potential was held at −0.43 V (Figure 4D), but the shapes of some dark patches have here started to convert from equi-triangular to irregular (e.g., indicated by a black arrow 5 in Figure 4E).

When the substrate potential was raised to a still slightly more positive value such as −0.41 V, the Au(111) surface becomes more active and mobile. As a consequence, many new dark sites rapidly emerge (e.g., indicated by 6, 7, and 8 in Figure 4F). The formation of dark patches was accelerated at −0.40 to −0.39 V, where the surface structure changed significantly (Figure 4G−H). The surface microscopic structures thus seem highly sensitive to the substrate potential with significant changes within small positive potential shifts (e.g., 10−20 mV). In addition to new patch sites emerging at the elbows (the black arrows 7 and 9 in Figure 4, panels G and H), the triangular dark patches continued to enlarge along the {11 $\bar{2}$} directions (indicated by the circle 6 in Figure 4G). At this stage, the shape of the dark patches becomes more diverse with different shapes coexisting on the surface. A similar tendency continues with expansion of dark patches and conversion of equi-triangular to irregular shapes as main features, Figure 4I. In contrast to previous observations of mercaptohexanol SAMs on Au(111) in UHV−STM by Poirier

(47) Nishizawa, M.; Sunagawa, T.; Yoneyama, H. *J. Electroanal. Chem.* **1997**, *436*, 213-218.
(48) Kolb, D. M. *Angew. Chem., Int. Ed.* **2001**, *40*, 1162−1181.

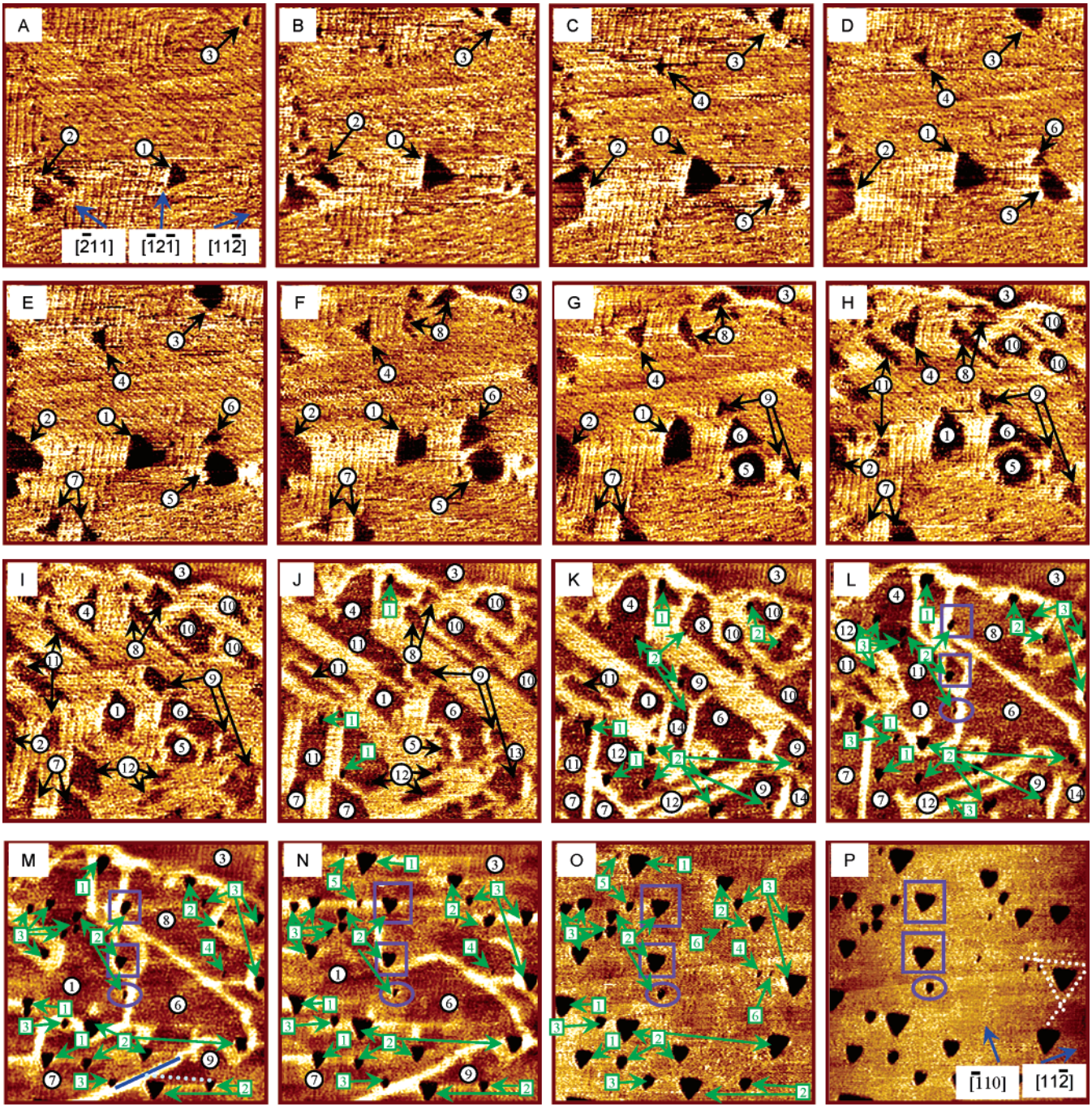

Figure 4. Sequence of in situ STM images for 1-propanethiol SAM formation on Au(111) in NH_4Ac buffer (5 mM, pH 4.6) containing 1.8 mM 1-propanethiol. Observations focused on the large terraces. $I_t = 0.15$ nA, scan area 180 × 180 nm^2. (A) $E_w = -0.48$ V (vs SCE), $V_{bias} = 0.13$ V, soaking time 3′31″. (B) $E_w = -0.45$ V, $V_{bias} = 0.10$ V, soaking time 4′55″. (C) $E_w = -0.45$ V, $V_{bias} = 0.10$ V, soaking time 5′37″. (D) $E_w = -0.43$ V, $V_{bias} = 0.08$ V, soaking time 6′19″. (E) $E_w = -0.41$ V, $V_{bias} = 0.06$ V, soaking time 7′01″. (F) $E_w = -0.41$ V, $V_{bias} = 0.06$ V, soaking time 7′43″. (G) $E_w = -0.40$ V, $V_{bias} = 0.05$ V, soaking time 8′25″. (H) $E_w = -0.39$ V, $V_{bias} = 0.04$ V, soaking time 9′07″. (I) $E_w = -0.39$ V, $V_{bias} = 0.04$ V, soaking time 9′50″. (J−P) $E_w = -0.38$ V, $V_{bias} = 0.03$ V; soaking times: (J) 10′32″, (K) 11′14″, (L) 11′56″, (M) 12′38″, (N) 13′20″, (O) 14′02″, and (P) 14′44″.

and co-workers,[11,26] we do not observe any "white" protrusions inside of patches with stronger electronic contrast (Figure 4A−I). This implies that a different mechanism is responsible for the 1-propanethiol SAM assembly from the solution under potential control.

A critical potential was reached at −0.38 V. As shown in Figure 4J−N, the number of new dark patches is very few. Instead, a rapid expansion of already existing dark patches was observed. This feature was unchanged by further shifting the substrate potential. The in situ observations were therefore focused on the time-dependent disappearance of reconstruction lines and formation of pits (pinholes or vacancy islands) at this potential. At these later stages, the rapid expansion of the dark patches resulted in fusion into larger patches, accompanied by the disappearance of the reconstruction lines (Figure 4J−N). Meanwhile, pits started to appear on the surface, indicated by the green arrows in Figure 4J. The initial sites of these pits are preferably located in the boundary regions between the dark patches and the joints of the reconstruction lines. The height of the pits is about 2.4 (±0.2) Å, corresponding to a mono-terrace of Au(111). This suggests

that a different process begins compared with the stages shown in Figure 4A−I. The population of pits is boosted by the appearance of many small new pits (the green arrows 2 and 3 in Figure 4, panels K and L). Apart from the pits located at the elbow sites, some new pits emerged along the reconstruction lines (e.g., a pit marked by a blue ellipse in Figure 4L). Notably, the development of the pits seems to depend on their initial locations. This is illustrated in a series of STM images in Figure 4L−P. For example, we could follow the evolution of three individual pits at two different kinds of sites. Two pits framed by blue rectangular boxes were located at the elbow sites, and one pit marked by a blue ellipse frame initially emerged in the middle of a reconstruction line. These three pits appeared at the same moment, but developed with significantly different speeds. The two pits at the elbow sites grew faster than the pit along the reconstruction line. Moreover, the two pits from the elbow sites evolved finally toward an equi-triangular shape with a larger size, whereas the third pit remained much smaller with an irregular shape. Other pits on the surface show similar features. The detailed observations from these three pits could thus be generalized up to a point; that is, the final size and shape of a pit are inherently determined by the site from which it initially emerges. Moreover, the edges of the triangular pits are either perpendicular to or 30° from the reconstruction lines. An example is shown by the dotted light blue line (the edge of a triangular pit) versus a solid dark blue line (the reconstruction line) in Figure 4M. This suggests that the triangular pits were generated along the atomic rows of the Au(111) substrate.

The formation of the 1-propanethiol SAM is thus accompanied by the disappearance of the reconstruction lines, the expansion and fusion of the dark patches, and the growth of the pits. These events are mutually dependent. Once the reconstruction lines are totally lifted (i.e., completed evolution of the dark patches), the number and size of the pits tend to be steady (Figure 4O−P). By detailed STM analysis, the total area occupied by all pits is estimated as 4.0 ± 0.4% of the whole SAM surface area. In this final stage, the Au(111) surface was fully covered by a 1-propanethiol monolayer. The detailed surface structure of the SAM can be imaged with molecular resolution as described below. The observations in Figure 4 thus suggest that the formation of the 1-propanethiol SAM follows two major steps. The first step (Figure 4A−I), termed "the weak-interaction step", is the initial lifting of reconstruction lines induced by the potential and the presence of 1-propanethiol. This step is highly and reversibly sensitive to the potential. This is further addressed below. The second step (Figure 4J−P), termed "the chemisorption step", involves mainly S−Au bond formation, accompanied by the creation of nanoscale pits. This step is an irreversible chemical process. The surface structures change dramatically toward the steady-state during the second step (e.g., Figure 4P), and the same clean reconstruction state (e.g., Figure 4A) cannot be recovered by setting the potential back to the starting point (−0.48 V). The transition between the two steps is determined by the potential and the concentration of 1-propanethiol and can be controlled by adjusting these parameters. The threshold potential is at −0.38 V with 1.8 mM 1-propanethiol, for example, but could change at different concentrations.

The adsorption dynamics thus depends on potential and thiol concentration. At lower 1-propanethiol concentrations the adsorption process initializes at more positive potentials than at higher concentrations. To demonstrate the reversibility of the first major step (or step I), we recorded in situ STM images with a 1-propanethiol concentration of 0.5 mM. This relatively low concentration is chosen, so that the first step prevails in a wider

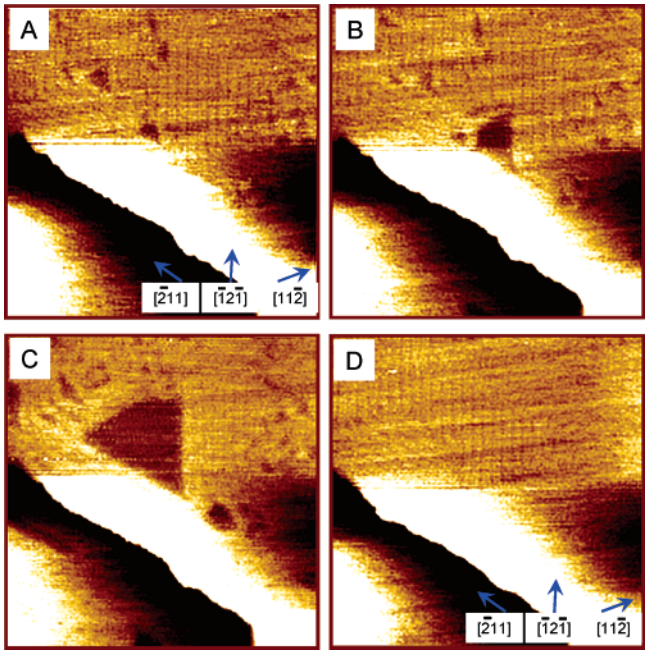

Figure 5. In situ STM images of the potential-dependent reversible lift of the Au(111) reconstruction lines in NH_4Ac buffer (5 mM, pH 4.6) containing 0.5 mM 1-propanethiol. Scan area: 180 × 180 nm^2, $I_t = 0.05$ nA, $V_{bias} = -0.10$ V. (A) $E_w = -0.21$ V (vs SCE), soaking time 11′13″. (B) $E_w = -0.16$ V, soaking time 12′38″. (C) $E_w = -0.16$ V, soaking time 14′24″, and (D) $E_w = -0.50$ V, soaking time 18′14″.

potential range and is easily controlled by the potential within a suitable time scale. The results are represented by a series of STM images in Figure 5 (more details are given in the Supporting Information, Figure S2). Figure 5A shows an STM image obtained at −0.21 V before the lift of the surface reconstruction. After acquiring the image (Figure 5A), the potential was gradually shifted positively. A dark triangular patch appeared at −0.16 V (Figure 5B). After about 46 s at this potential, the triangular patch expanded along the reconstruction lines to a significantly larger size (Figure 5C). In addition, many small new dark patches emerged. These observations are clearly similar to those in Figure 4A−I, and a notable signature for the first step of the whole process. When the potential was set back to negative values (e.g., at −0.50 V), all dark patches completely vanished and the herringbone-like reconstruction lines were fully recovered (Figure 5D). This experiment thus shows that the first major step is a potential-dependent reversible process.

Formation of 1-Propanethiol SAMs at Au(111) Terrace Edges. The adsorption patterns at the terrace edges and within the large terraces are notably distinct. Figure 6 shows a series of images during 1-propanethiol adsorption with focus on the edge regions (more details are given in the Supporting Information, Figure S3). Figure 6A shows that clean Au(111) terraces with reconstruction lines dominate at the low potential −0.48 V in the presence of 1.8 mM 1-propanthiol, i.e., the same experimental conditions as for Figure 4A. Smooth terrace edges were observed at this potential. When the potential was shifted positively to −0.43 V, corresponding to the same conditions as for Figure 4C, a series of time-dependent changes were observed (Figure 6B−L). Similar to the observations in Figure 4, many small dark patches indicated by circle 1 among the reconstruction lines and some small ripples on the edge of the top terrace started to emerge (Figure 6B). The area of these dark patches increased and some new small patches were formed (Figure 6C). At the same time, shape evolution of the ripples on the terrace edge began. The

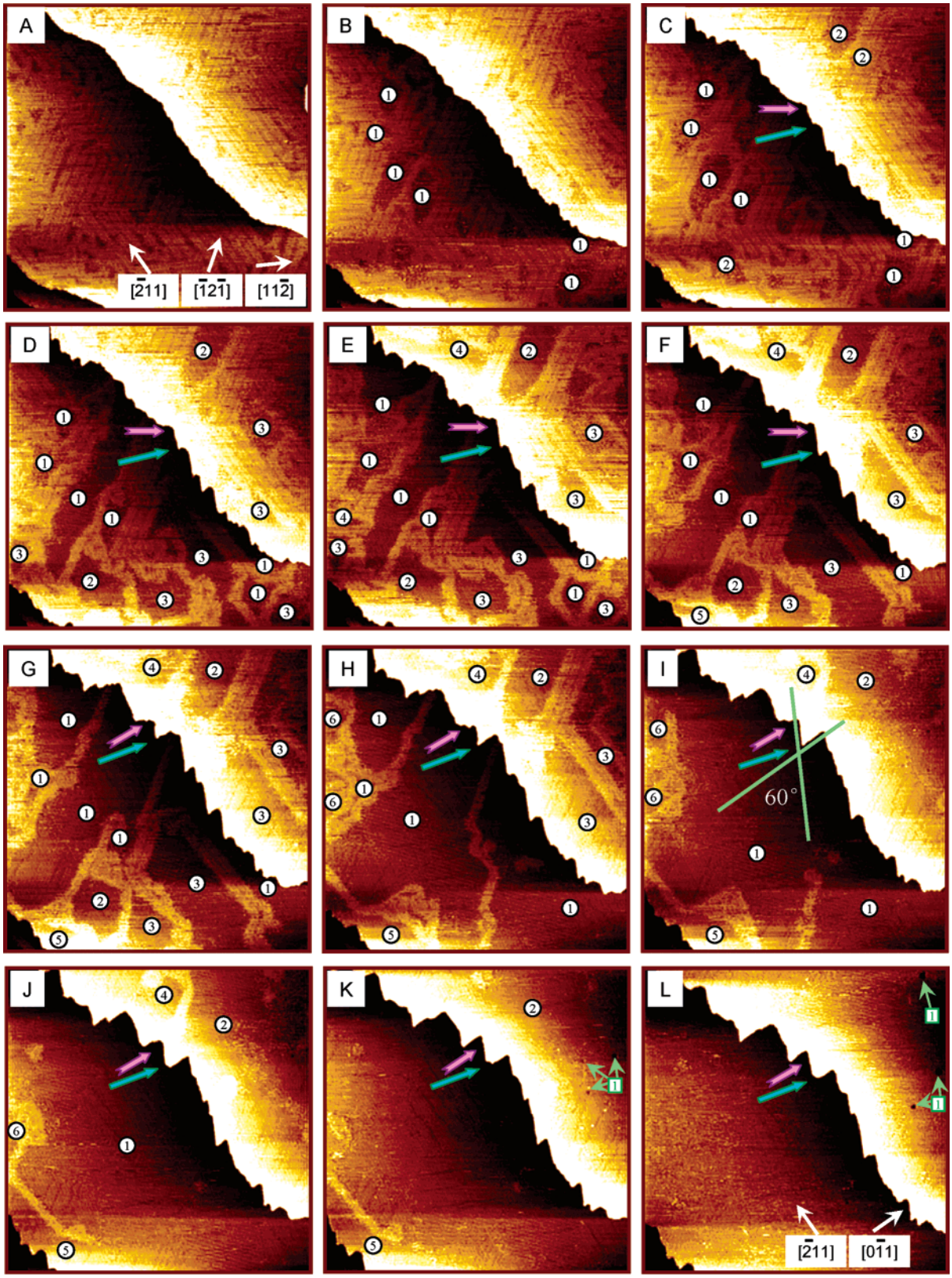

Figure 6. Sequence of in situ STM images for 1-propanethiol SAM formation on Au(111) in NH_4Ac buffer (5 mM, pH 4.6) containing 1.8 mM 1-propanethiol. Observations focused on the terrace edges. $I_t = 0.15$ nA, scan area 190 × 190 nm^2. (A) $E_w = -0.48$ V (vs SCE), $V_{bias} = 0.22$ V, soaking time 0′59″. (B−L) $E_w = -0.43$ V, $V_{bias} = 0.17$ V, soaking times: (B) 2′11″, (C) 2′55″, (D) 3′24″, (E) 3′53″, (F) 4′22″, (G) 4′51″, (H) 5′20″, (I) 5′49″, (J) 6′18″, (K) 6′48″, and (L) 8′15″.

ripples first had a "zigzag-shape" and then gradually developed into well defined shapes. A peninsula-like patch and a dented structure are indicated by blue and red arrows in Figure 6, panels C and D, respectively. Both the area and density of the dark patches increased as expected, whereas the changes at the terrace edges became even more pronounced (see Figure 6, panels D and E). The dark patches fused together to form larger patches within the terraces, while the terrace edges evolved into many

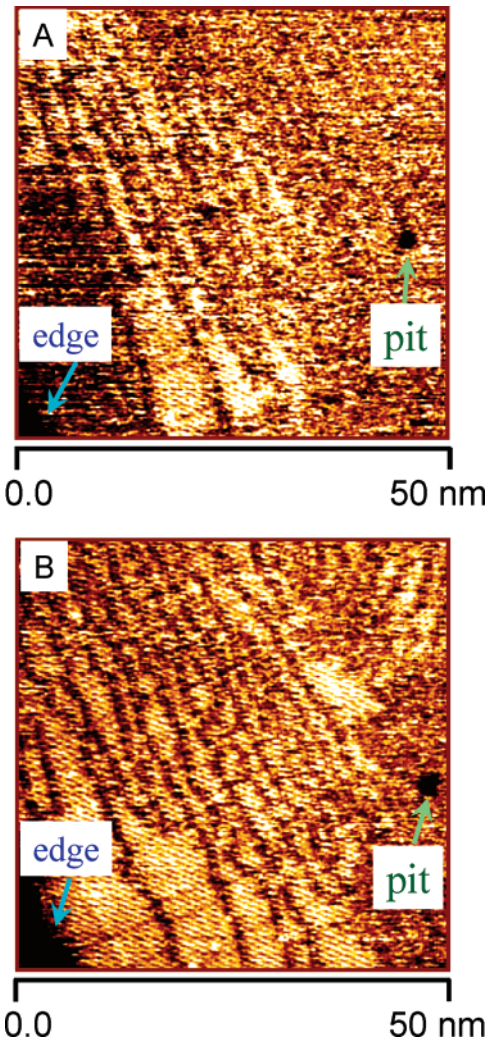

Figure 7. In situ STM images of partially covered 1-propanethiol monolayer on Au(111) in NH_4Ac buffer (5 mM, pH 4.6) containing 1.8 mM 1-propanethiol. Observations focused on a terrace edge. Scan area: 50×50 nm^2; $I_t = 0.20$ nA, $V_{bias} = 0.16$ V, $E_w = -0.43$ V (vs SCE). Soaking time: (B) is 2 min more than (A).

small peninsulae with a tooth-like shape (Figure 6, panels F and G). At this stage, the dark patches were covered by a highly ordered 1-propanthiol SAM, even though the surface reconstruction was not completely lifted (Figure 6, panels G and H). On the other hand, the peninsulae at the terrace edges continued to evolve toward a well-defined triangular shape, as illustrated by the blue and red arrows in Figure 6H. The angle between the peninsula sides was measured as $60 \pm 5°$ (e.g., green lines in Figure 6I). We found by further analysis that these sides are parallel to the Au(111) atomic row directions. The final stages of the surface evolution are shown in Figure 6J−K. Similarly to Figure 4, the formation of the SAM close to the terrace edges was completed with full lift of the reconstruction lines. However, there are much fewer and smaller (only 2−4 nm in diameter) pits in the SAM around the terrace edges, compared to the SAMs on the larger terraces (cf. Figure 4). The terrace edge had a sawtooth-like shape with a sharp fringe (Figure 6I) that finally changed into a smooth fringe (Figure 6L).

For more details, we further observed the time-dependent development of the 1-propanethiol SAM at a terrace edge (ca 50 nm × 50 nm). Figure 7 shows two such observations. An early stage of the SAM growth was imaged in Figure 7A; that is, the whole surface was partially covered by 1-propanethiol. The 1-propanethiol coverage at this stage is higher at the edge than within the terrace. This indicates that the SAM formation is energetically favored at the edge. After an additional 2 min, the edge was fully covered with 1-propanethiol but the terrace was only partially covered. This suggests that the growth of the SAM at the edge is also faster (Figure 7B). In addition, in contrast to the observations in Figure 4, the pit indicated by the green arrow was only slightly enlarged but did not evolve into a triangular shape.

In summary, under the present experimental conditions 1-propanethiol can be assembled into a highly ordered monolayer on the Au(111) surface at both the terrace edges and inside terraces, accompanied by lifting of the surface reconstruction. Different adsorption patterns at the terrace edges and within the terraces are observed (compare Figures 4 and 6), the main differences being as follows: (1) A notable number of triangular pits are observed within the large terraces during thiol assembly, but with no such triangular pits at the terrace edges. Instead, only few and small pits with irregular shapes were observed. The edges were, moreover, converted from a smooth shape into well-defined sawtooth-like fringes. (2) At a given 1-propanethiol concentration, less energy is needed for 1-propanethiol adsorption at the terrace edge than within the terrace. This is reflected by the different potentials required for SAM growth. The potential applied in Figure 6B−L is −0.43 V, but a more positive potential (−0.38 V) was needed for the images in Figure 4J−P. The SAM formation at the edge areas can be completed at −0.43 V, but at this potential (−0.43 V), the reconstruction lines within the terraces are only partially lifted within the same time scale, and the SAM formation was far from completion.

High-Resolution Lattice Structure of 1-Propanethiol SAMs. After completion of the 1-propanethiol SAM formation, the surface contains ordered domains, domain boundaries, and pits scattered over the SAM. These components are commonly found in alkanethiol SAMs. STM enables disclosure of the detailed lattice structure of the ordered SAM domains. Figure 8A shows highly ordered domains as well as nanoscale pits. The angles between the domains are 60° or multiples of 60°, i.e., following the 3-fold symmetry of the Au(111) surface. The nanoscale pits (especially the larger ones) are mostly located at the domain boundaries. The size of most domains is in the range of 20−40 nm. A STM image with molecular resolution within an ordered domain is shown in Figure 8B. There are two kinds of spots with significantly different contrast. The spots are distributed along the Au(111) atomic rows to form a highly ordered lattice. The periodic distance along the Au(111) atomic row is 8.7 ± 0.3 Å, corresponding to three times the diameter of a gold atom. The periodic distance in the perpendicular direction is 10.2 ± 0.3 Å, equal to $2\sqrt{3}$ times the diameter of a gold atom. A unit cell consisting of one brighter and three weaker spots is therefore assigned as $(2\sqrt{3} \times 3)$R30°, indicated by a blue box in Figure 8B. The $(2\sqrt{3} \times 3)$R30° lattice gives a surface coverage of 1.92×10^{-10} mol cm^{-2}. The 1-propanethiol SAM surface coverage measured from reductive desorption is $7.6 (\pm 0.5) \times 10^{-10}$ mol cm^{-2} (Figure 2), i.e., about four times the theoretical value for the $(2\sqrt{3} \times 3)$R30° surface lattice. This combination suggests that each unit cell contains four individual 1-propanethiol molecules, and each spot with either stronger or weaker contrast represents a single 1-propanethiol molecule. As a result, the lattice structure of the 1-propanethiol SAM can be described as $(2\sqrt{3} \times 3)$ R30°-4. This structure is a variant of the classic $(\sqrt{3} \times \sqrt{3})$R30° lattice for alkanethiol SAMs.

Figure 9 shows a simple surface model to account for the STM image in Figure 8B. The empty and filled circles in Figure

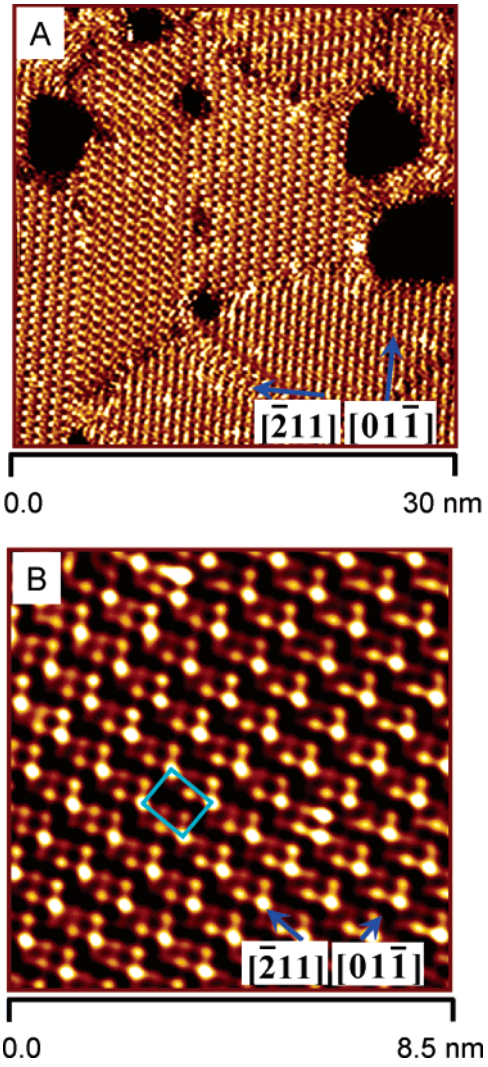

Figure 8. High-resolution in situ STM images of 1-propanethiol SAM on Au(111) in NH_4Ac buffer (5 mM, pH 4.6). Scan area: (A) 30×30 nm^2 and (B) 8.5×8.5 nm^2. (A) $I_t = 0.30$ nA, $V_{bias} = -0.13$ V, $E_w = -0.07$ V (vs SCE); and (B) $I_t = 0.30$ nA, $V_{bias} = 0.07$ V, $E_w = -0.15$ V.

9A represent, respectively, gold atoms and 1-propanethiol molecules. As noted, the different contrasts in the STM image (Figure 8B) most likely reflect adsorbed molecules in different configurations, resulting in different apparent conductivities.[49,50] We use pink and blue filled circles in Figure 9A to denote stronger- and weaker-contrast spots, respectively. Two configurations of a 1-propanethiol molecule give different tunneling pathways (Figure 9B). For example, an upright configuration (left in Figure 9B) gives more facile tunneling than a bending-down configuration (right in Figure 9B). The upright configuration could therefore correspond to the stronger contrast, whereas the bent-down configuration gives the STM spots with a weaker contrast. The top views of these two configurations are here simplified by round circles but are actually different in structural detail. In Figure 9A, we assume that four molecules with the upright configuration (red filled circles) are confined on 3-fold sites in the four corners of a $(2\sqrt{3} \times 3)$R30° unit cell, whereas three molecules with the bent-down configuration (blue filled circles)

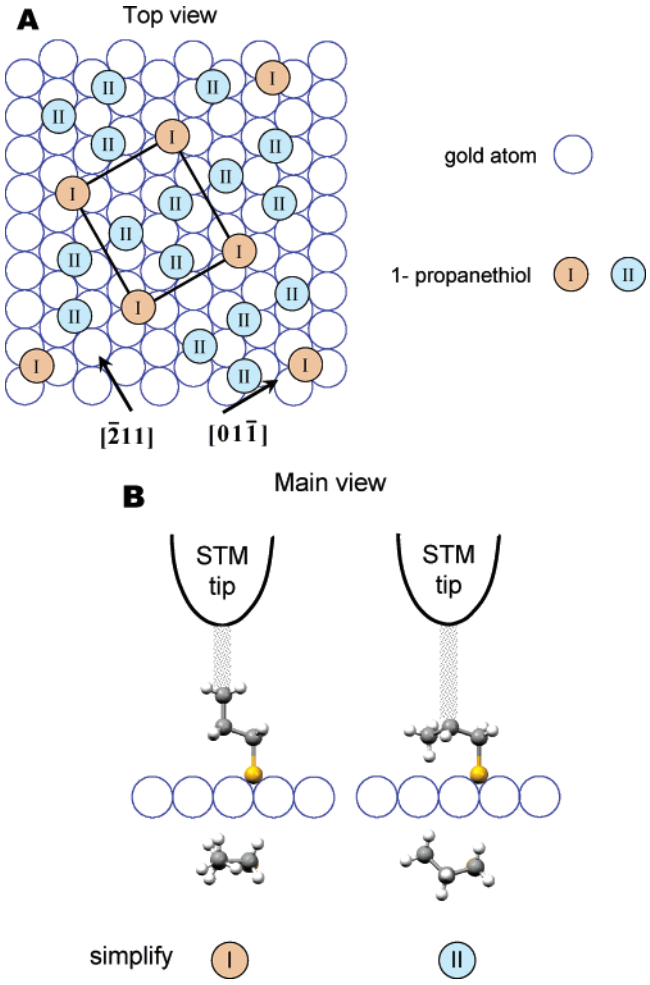

Figure 9. (A) Possible surface model for a $(2\sqrt{3} \times 3)$ R30° unit cell containing four 1-propanethiol molecules, and (B) a proposed illustration of two configurations of adsorbed 1-propanethiol and corresponding tunneling pathways.

are located on 2-fold bridge sites. This model thus implies three bent-down molecules and one upright molecule composing a $(2\sqrt{3} \times 3)$ R30° unit cell, consistent with the surface lattice structure in Figure 8B. Theoretical and computational inputs are desirable to quantify these observations such as recently achieved for cysteamine[17] and cysteine SAMs on Au(111).[51] On the other hand, AFM can measure direct height on the SAMs, but so far the resolution of AFM is hard to achieve the same level as STM. With the developments of AFM technique, it will be very interested to directly compare images from both STM and AFM at the molecular level.

Discussion

Origin of Nanoscale Pits in the SAMs. Regardless of the preparation methods, pits in thiol SAMs (also called vacancy islands (VIs) of gold atoms) have long been observed. [13,17,22,38] However, the mechanism of pit formation has not been clarified. Three possible mechanisms have been proposed, based on a variety of evidence obtained under different experimental conditions. Edinger et al. proposed chemical etching of the gold surface in alkanethiol-containing solutions.[52] This was supported mainly by atomic absorption spectroscopy that showed the existence of dissolved Au in the incubation solution.[52] The second mechanism suggested that pit formation originates in compression

(49) Moth-Poulsen, K.; Patrone, L.; Stuhr-Hansen, N.; Christensen, J. B.; Bourgoin, J. P.; Bjørnholm, T. *Nano Lett.* **2005**, *5*, 783−785.
(50) Meyer, E.; Hug, H. J.; Bennewitz, R. *Scanning probe microscopy*; Springer-Verlag: Berlin, 2004.
(51) Nazmudtinov, R. R.; Zhang, J.; Zinkicheva, T. T.; Manyurov, I. R.; Ulstrup, J. *Langmuir*, accepted.

of the surface lattice; that is, the VIs were formed through shrinking of the gold surface lattice constant induced by the alkanethiols.[11] In the third mechanism, gold VIs are assumed to be generated by specific ejection of compressed gold atoms in the reconstructed state. The third mechanism was based only on UHV−STM observations.[22,23] The present in situ STM observations suggest that pit formation is most likely due to shrinking of the gold atoms in the top layer of the surface first and rearrangement of these atoms at a later stage.

From in situ STM visualization of the SAM formation shown in Figure 4, the pit formation was initialized while the reconstruction lines were still only partially lifted (Figure 4J) and reached a maximum once the SAM assembly was completed (Figure 4, panels O and P). Moreover, most pits have a well-defined triangular shape following the Au(111) atomic rows with no protrusions along the *z* direction (Figure 4I−K). These observations are clearly different from those in UHV−STM.[22,23] If the ejection mechanism applies, the total area occupied by the pits should be the same as for the protrusions. This is unlikely, since protrusions found by STM are significantly smaller than the pits in the total area, even for alkanethiol SAM formation in UHV.[22−24] Similarly, chemical etching can hardly explain the fact that the surface coverage of the pits did not change once the SAM formation was completed. On the other hand, gold atoms in their neutral state have a diameter of 2.88 Å, whereas the diameter of positively charged gold ions (Au^+) is 2.74 Å. The gold covalent radius is 1.34 Å. Gold atoms on clean bare Au(111) surfaces are commonly regarded as being in neutral state with 2.88 Å in diameter. However, although the diameter of gold atoms in the reconstructed state is still 2.88 Å in the $\sqrt{3}$ direction and 2.77 Å in the atomic direction, since the gold atoms along the atomic row direction are compressed by 4% in order to form the $(\sqrt{3} \times 22)$R30° lattice (Figure 3). The assembly of alkanethiols on the gold surface is based on formation of the Au−S bonds. In the Au−S bonds, gold is no longer neutral but approaches Au^+, because the adsorbate is in the thiolate state as measured by XPS.[19] This means that gold atoms shrink from 2.88 Å to either 2.68 Å for a covalent Au−S bond or to 2.74 Å for a Au^+S^--R unit during the SAM formation.

According to the model in Figure 9, each unit cell for the $(2\sqrt{3} \times 3)$R30°-4 surface lattice contains 12 gold atoms and 4 1-propanethiol molecules. One-third of the surface gold atoms could thus shrink from 2.77 Å in the atomic rows (or 2.88 Å in the perpendicular directions, i.e., $\sqrt{3}$ direction) to 2.68 Å, giving rise to a total shrinking of 3.4% of the whole surface. We therefore suggest that the shrinking mechanism best fits our experimental observations for pit formation, particularly the following three features: (1) the pits were formed during thiol assembly. (2) The pits were formed by the lifting of the reconstruction lines. The area and density of the pits increased to a maximum once the whole surface was covered by the SAMs. The total area of the pits was estimated experimentally as 4.0 (± 0.4) % of the whole surface area, largely consistent with the calculation from the shrinking model (3.4%). (3) The pit shape is determined largely by the shrinking of gold atoms along the Au(111) atomic rows, resulting in most pits having a triangular shape.

Possible Mechanism of the Shape Changes at Terrace Edges. The 1-propanethiol SAM assembly is accompanied not only by pit formation (Figure 4) but also by significant structural changes at the terrace edges (Figure 6). The terrace edges changed from a smooth shape into sawtooth-like fringes (Figure 6). At first sight, the saw-like teeth seem to be generated by potential-induced etching in the presence of 1-propanethiol. However, this can hardly account for the triangular shape of the saw-like teeth particularly along the Au(111) atomic rows (Figure 6, panels H and I). Furthermore, this view cannot explain the observation that only few and small pits are formed at the terrace edges. Following the interpretation of pit formation above, we suggest that shrinking and rearrangement of gold atoms are also responsible for structural changes at the terrace edges. Gold atoms at the terrace edges are more active and mobile and consequently more easily rearranged than gold atoms inside the terraces. It is thus not surprising that shrinking and rearrangement of gold atoms at terrace edges can reach a higher degree than inside the terraces. The more profound shrinking might thus compensate for lower density and smaller pit size at the terrace edges, if a constant total shrinking of gold atoms is required during the SAM formation.

Relative Contrast in STM Images. Figures 4−7 not only illustrate the dynamic adsorption processes of the 1-propanethiol SAM but also a fundamental puzzle, i.e., the primary factors that determine the apparent height in STM images acquired in the constant current mode. Objects with higher physical height are closer to the STM tip and intuitively expected to generate a larger tunneling current (i.e., stronger contrast). In the constant current mode, the STM tip therefore retracts vertically and gives a larger apparent height.[50] This expectation seems to apply to UHV−STM for mercaptoethanol SAMs on Au(111),[22,23] the SAM domains of which showed a stronger contrast (i.e., brighter) than herringbone-like reconstruction lines. This is, however, in contrast to the present in situ STM observations at liquid /solid interfaces. The bare Au(111) surface with reconstruction lines gives a brighter contrast than the patches covered by 1-propanethiol. This is pronounced in some intermediate states of the adsorption process, where the gold surface is partially covered by a 1-propanethiol SAM, cf. Figure 6H. The 1-propanethiol monolayer is located on the dark patches, whereas the rest of the reconstruction lines indicating bare Au(111) give a brighter contrast. This observation suggests that, even with a higher physical height, the area covered by the 1-propanethiol SAM appears "electronically lower" than the bare Au(111) substrate. A possible interpretation is that gold is more conducting than organic molecules. However, the reason that the observations in UHV and in solution are dramatically different remains a puzzle. Extensive theoretical and computational inputs are needed to disentangle this puzzle.

Concluding Summary

The present work has combined electrochemistry and in situ STM to map the structure and dynamics of 1-propanethiol SAMs on Au(111) with nanoscale and molecular resolution. Electrochemistry has shown that 1-propanethiol forms large and dense SAMs on Au(111) in suitable concentration ranges. High-resolution STM images have revealed a $(2\sqrt{3} \times 3)$R30° surface periodic lattice with each unit cell containing one brighter and three weaker spots. Together with the coverage measured from reductive desorption, each spot is confirmed to represent a single 1-propanethiol molecule. We suggest that the different STM contrasts arise from upright and bent-down configurations of adsorbed 1-propanethiol. The potential-dependent adsorption dynamics has been visualized in real time by in situ STM. The observations, including growth of the SAM domains, lifting of reconstruction lines, and pit formation, have reached a high level of detail. We have also proposed a mechanism or model to interpret the observations and suggest that shrinking and

(52) Edinger, K.; Golzhauser, A.; Demota, K.; Woll, Ch.; Grunze, M. *Langmuir* **1993**, *9*, 4−10.

rearrangement of gold atoms are most likely responsible for pit formation in the SAMs and for structural changes at the terrace edges.

The results are of fundamental interest by pointing to the degree of detail in molecular adsorbate structure and dynamics. The adsorbate structure mapped to nanoscale or molecular resolution has enabled us to identify several stages in the time evolution of the adsorption process characterized with comparable resolution. Solid−liquid interfacial structure and dynamics at this level of resolution are likely to offer useful information in some areas of pure and applied science, such as molecular and electronic structures of solid−liquid interfaces, novel views of catalytic surfaces, biomolecular immobilization with chemical and biological functionality retained, and external control of functionalized surfaces down to the single-molecule level.

Acknowledgment. Financial support from The Danish Research Council for Technology and Production Sciences (Contract No. 26-00-0034) is acknowledged.

Supporting Information Available: Molecular structure of 1-propanethiol (Figure S1), additional STM images for reversible lifting of the Au(111) reconstructed structure (Figure S2), and 1-propanethiol SAM formation on the terrace edges (Figure S3). This material is available free of charge through the Internet at http://pubs.acs.org.

LA0605891